arXiv:1412.1617v1 [cond-mat.soft] 4 Dec 2014

Heirarchical Self Assembly: Self Organized nano-structures in a nematically ordered matrix of self assembled polymeric chains.

Shaikh Mubeena, Apratim Chatterji*

IISER-Pune, 900 NCL Innovation Park, Dr. Homi Bhaba Road, Pune-411008, India.

(Dated: December 5, 2014)

We report many different nano-structures which are formed when model nano-particles of different sizes (diameter σ_n) are allowed to aggregate in a background matrix of semi-flexible self assembled polymeric worm like micellar chains. The different nano-structures are formed by the dynamical arrest of phase-separating mixtures of micellar monomers and nano-particles. The different morphologies obtained are the result of an interplay of the available free volume, the elastic energy of deformation of polymers, the density (chemical potential) of the nano-particles in the polymer matrix and, of course, the ratio of the size of self assembling nano-particles and self avoidance diameter of polymeric chains. We have used a hybrid semi-grand canonical Monte Carlo simulation scheme to obtain the (non-equilibrium) phase diagram of the self-assembled nano-structures. We observe rod-like structures of nano-particles which get self assembled in the gaps between the nematically ordered chains as well as percolating gel-like network of conjoined nanotubes. We also find a totally unexpected interlocked crystalline phase of nano-particles and monomers, in which each crytal plane of nanoparticles is separated by planes of perfectly organized polymer chains. We identified the condition which leads to such interlocked crystal structure. We suggest experimental possibilities of how the results presented in this paper could be used to obtain different nano-structures in the lab.

PACS numbers: 81.16.Dn,82.70.-y,81.16.Rf,83.80.Qr

There is persistent interest in the controlled self assembly and growth of nano-structures of predefined morphology and size starting from small constituent nanoparticles (NP) [1–29]. A separate non-alligned interest of physicists is in the formation and properties of topological defects when large particles (large compared to the size and spacing between nematogens) are introduced in ordered liquid crystalline nematic and smectic phases [29–41]. Recents experiments have also explored the self organization of nano-particles in a background matrix of nematically ordered micellar phase, but constraints in the choice of size of NPs led to the following two scenarios: small NPs of $2-3$ nm diameter pervade the nematic chains themselves and form a dispersion/solution, whereas, larger NPs of size $8-26$ nm get expelled by the elastic energy of ordered nematic phases and aggregate at the grain boundaries between nematic domains [42–44]. The distance between adjacent nematic chains was 5.7 nm in the experiments.

Our present study spans across these two different research domains and we use computer simulations to investigate the heirarchical self assembly of NPs in the free volume between parallel chains of nematically ordered worm-like micelles (WM). The micellar polymers are self-assembled themselves from monomeric beads and have a length and size distribution controlled by monomer density and temperature [45–47]. In a computer simulation, we are able to systematically vary the diameter, chemical potential of the spherical NPs as well as the excluded volume (EV) of self-avoiding semiflexible chains in the matrix of the NPs self-organize. Thereby, we observe the effect of the above parameters, as well as the elasticity of the background micellar matrix on the morphology and size of the NP-nano-structures. The nanostructured aggregates in turn increase the effective density of monomers constituting the background matrix and make them more nematically ordered with longer chains spanning the length of the system.

At suitable densities and radii of NPs we get rod like aggregates of different aspect ratios shaped by the geometry of the background matrix: EV and elastic energy costs of accomodating the NPs amongst the semiflexible polymeric micelles encourage the NPs to form aggregates even at moderate number densities. Since the background matrix is not only deformable but also prone to scission and recombination, neighbouring rod-like aggregates of NPs can also fuse at times forming porous percolating networks of extended tubular structures. In experimental realizations of our studies, these nano-structures could be stable due to van der Waals attraction even if the background micellar matrix is dissolved away by adding suitable ions in solution by reverse-micellization as in [48, 49]. To our surprise, we also get a perfectly crystalline phase spanning the simulation box where both NM and the WM forming monomers form alternate lines of NP and monomers forming a closed packed structures. In the following we describe the model of (a) self assembling WM chains (b) the NP and (c) the polymer-NP interaction. We then describe the different nano-structures obtained and summarize the conditions under which the

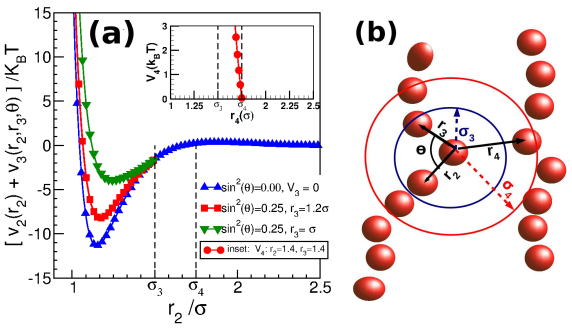

FIG. 1. (a) shows a plot of the two body and three body potential between 2 monomers $V_2(r_2) + V_3(r_2, r_3)$; r_2 (r_3) is the distance between monomer 1 and 2 (1 and 3). Refer (b) for a schematic diagram for r_2, r_3, r_4, θ and σ_3, σ_4. The inset figure in (a) shows the repulsive potential V_4 on a fourth monomer for distance $r_4 < 2^{1/6}\sigma_4$ from central particle. Note $\sigma_4 > \sigma_3$.

different assembled structures are formed.

The unit of length for our simulations is the diameter σ of monomers which self assemble to form worm-like *equilibrium* polymers at a temperature k_BT; we set k_BT to be the unit of energy. The interaction potential between neighbouring monomers is the sum of two body and three body terms, V_2 and V_3, respectively, with $\epsilon = 110k_BT$:

$$V_2 = \epsilon[(\frac{\sigma}{r_2})^{12} - (\frac{\sigma}{r_2})^6 + \epsilon_1 e^{-ar_2/\sigma}]; \forall r < r_c. \quad (1)$$

$$V_3 = \epsilon_3(1 - \frac{r_2}{\sigma_3})^2(1 - \frac{r_3}{\sigma_3})^2 \sin^2(\theta); \forall r_2, r_3 < \sigma_3. \quad (2)$$

Here r_2 (r_3) is the distance between monomers 1&2 (monomers 1&3), the exponential term in Eqn.1 creates a maxima in the $V_2(r)$ at $r \approx 1.75\sigma$ (refer Fig.1a); we set $r_c = 2.5\sigma$, $\sigma_3 = 1.5\sigma$ and define σ_3 to be the cut-off distance above which the bond between monomers is considered broken. The 3-body interaction $V_3(r_2, r_3)$, which models semiflexibility of chains, sets in only when a monomer has at least two bonded neighbours at distances $r_2, r_3 < \sigma_3$ (see Fig1b). The angle θ is subtended between $\vec{r_2}$ and $\vec{r_3}$. We set $\epsilon_1 = 1.34\epsilon$, $\epsilon_3 = 6075k_BT$ and $a = 1.72$. A string of monomers can line up and form a chain and the value of ϵ_3 determines the measure of semi-flexibility of a chain. The squared terms which are a prefix to $sin^2(\theta)$ in Eqn 2 ensure that the potential and the force go smoothly to zero as either of r_2/σ_3 or $r_3/\sigma_3 \to 1$. Note in Fig.1a that the effective depth of the potential is a few times k_BT and depends on an interplay between V_2 and V_3.

To prevent branching, we ensure that a fourth monomer does not approach a triplet of monomers and is repulsed by a additional potential $V_4(r_2, r_3, r_4)$, if the distance r_4 between the central monomer and the fourth monomer becomes less than σ_4. We choose $\sigma_4 = 1.75\sigma$.

$$V_4 = \epsilon_4(1 - \frac{r_2}{\sigma_3})^2(1 - \frac{r_3}{\sigma_3})^2 \times V_{LJ}(\sigma_4, r_4) \quad (3)$$

$\forall r_4 < 2^{1/6}\sigma_4$, and $\forall r_2, r_3 < \sigma_3$. Here $V_{LJ}(\sigma_4, r_4)$ provides purely repulsive interaction between monomers 1 and 4 by a suitably shifted and truncated Lennard Jones (LJ) potential. The expression for V_{LJ} is $(\sigma_4/r_4)^{12} - (\sigma_4/r_4)^6$. The large value of $\epsilon_4 = 2.53 \times 10^5 k_B bT$ ensures sufficient repulsion even when both $(1 - r_2/\sigma_3)^2$ and $(1 - r_3/\sigma_3)^2 \approx 0.01$; this corresponds to $r_2/\sigma_3 = 0.9$ and $r_3/\sigma_3 = 0.9$. We explicitly checked that the chains do not have branches. The extra V_4 potential and the modified terms in Eqn. 2 improves upon the previous potentials used to model equilibrium polymers [50–53].

Figure 2a and 2b shows snapshots of 6000 and 7500 monomers, respectively, in a $30 \times 30 \times 60\sigma^3$ simulation box after the system is equilibrated using Monte Carlo (MC) Metropolis algorithm. The low density equilibrium configuration is a disordered isotropic phase with small chains. We have checked that an exponential distribution of chain lengths is obtained [45]. To obtain the nematically ordered phase with long chains as shown in Fig. 2b, we have used a symmetry breaking field B_n which adds an energy $E_B = -(\hat{r}_2 \cdot \vec{B}_n)^2$ to the Hamiltonian; B_n acts only if $|\vec{r}_2| < \sigma_3$. We use $B_n^2 = 0.025k_BT/a^2$, which biases $\vec{r}_2$ to allign along $\hat{z}$.

In Figure 2 c, d and e we have identified the range of densities over which the isotropic to nematic (I-N) transition occurs by plotting the average energy $\langle E \rangle$ of the monomers, the nematic order parameter $s = \langle 3\cos^2(\phi) - 1/2 \rangle$ and the average length of chains $\langle L \rangle$ as a function of number density ρ of monomers. The angle ϕ is the angle between a bond vector connecting adjacent monomers in a chain and $\hat{z}$. All the quantities show a sharp increase/decrease at the transition, i.e., for values of $\rho > 0.12\sigma^{-3}$. An increase in σ_4, which increases the volume excluded by the chains, makes the transition sharper and also shifts it to lower densities. To assure ourselves of the robustness of our results, we carried out simulation for $B_n^2 = 0.1k_BT/\sigma^2$ as well as lower value of $B_n^2 = 0.025k_BT/a^2$ in boxes of $30 \times 30 \times 30\sigma^3$ and $30 \times 30 \times 60\sigma^3$, respectively. A previous detailed study using a potential similar to this model had established a weakly first order isotropic to nematic phase transition [50]. We can use the term V_4 to vary EV of chains, and avoid branching even for MD simulations. We maintain $\rho = 0.126a^{-3}$ (6800 monomers) at the I-N transition with $\sigma_4 = 1.75\sigma$ in a box of $30 \times 30 \times 60\sigma^3$ and the $B_n^2 = 0.1k_BT/\sigma^2$ fixed, for results presented hereafter.

To study NP microstructure formation in a matrix of nematic polymers, we start introducing NPs amidst preformed nematically ordered chains. The monomers self assemble into ordered WMs within 10^5 MC steps starting from a random initial configuration of 6800 monomers and 100 NPs. Then we attempt to add (remove) randomly chosen NPs 300 times every 50 MC steps for the next 19×10^5 MC steps. In one MC step, we attempt to change the position of all particles present by δ_i, δ_i is a random number between 0 and 0.25σ and $i \in x, y, z$.

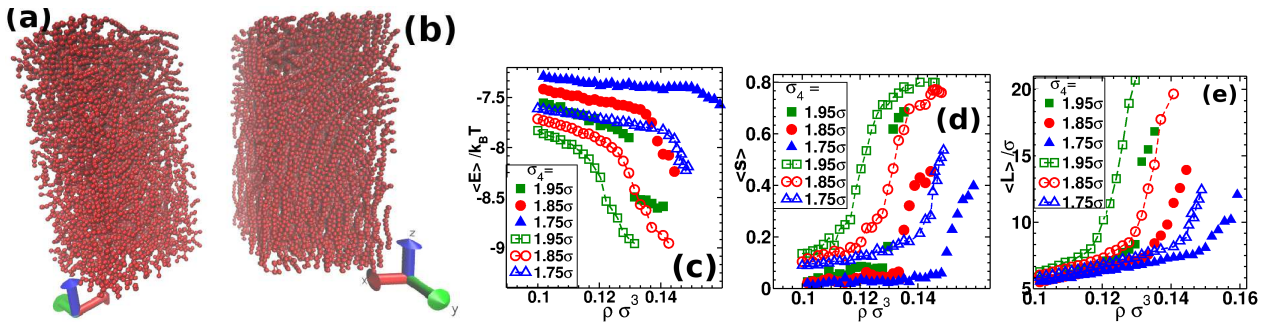

FIG. 2. Representative snapshots of (a) isotropic and (b) nematically ordered phase of self-assembling monomers forming worm-like micelles(WM). The number of monomers are 6000 and 7500, respectively, in a $30\times30\times60\sigma^3$ box for a small symmetry breaking field $B_n^2 = 0.025k_BT/\sigma^2$ and $\sigma_4 = 1.95\sigma$. To identify the isotropic-nematic transition densities plots of average energy $\langle E\rangle$, average length $\langle L\rangle$ and the nematic order parameter $\langle s\rangle$ versus the number density $\rho\sigma^{-3}$ is shown in subfigures (c),(d) and (e), respectively. Data is shown for $B_n^2 = 0.025k_BT/\sigma^2$ (filled symbols) and $0.1k_BT/\sigma^2$ (empty symbols).

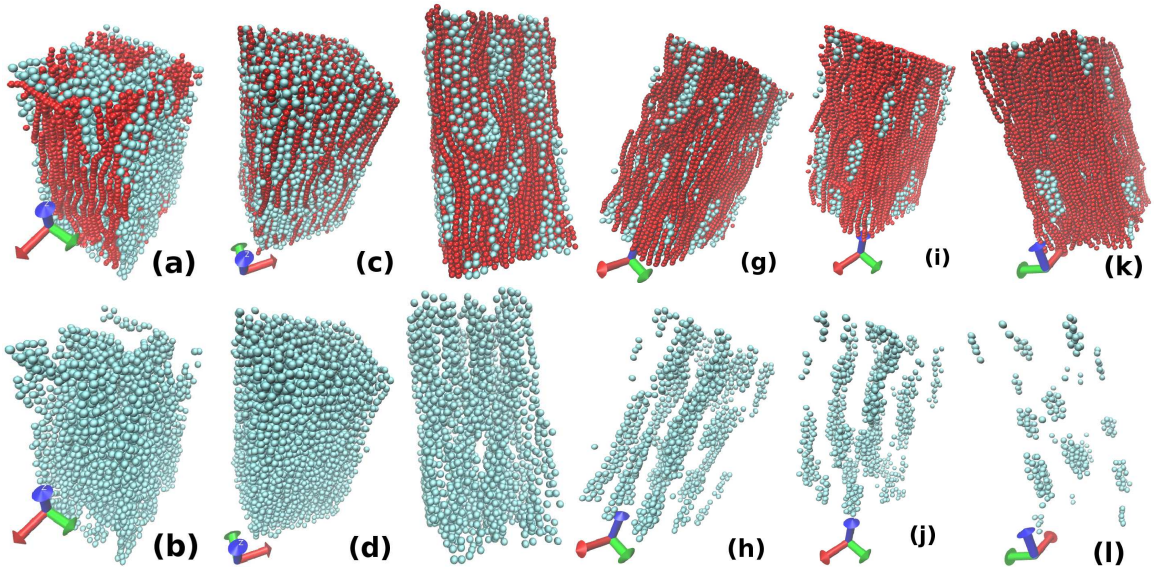

FIG. 3. Snapshots of WM chains (red) and structures formed by aggregates of nano particles-NP (blue) are shown. The snapshots in b, d, f, h, j, l are exactly the same snapshots of a, c, e, g, i, k, with monomers made invisible to have unhindered view of NPs. (a) and (b) show an equilibrated phase separated configuration with 4200 monomers and $\mu = -0.48k_BT$ and $\epsilon_n = 10k_BT$ for NPs with $\sigma_n = 2\sigma$ and $\sigma_{4n} = 1.75$ in a $30\times30\times60\sigma^3$ box. Snaphots (c) to (l) show dynamically arrested configurations of monomers and NPs; for these the values of μ, ϵ_n and the NP radius σ_n is kept fixed at $16k_BT, 14k_bT$ and 2σ, respectively. But $\sigma_{4n} = 1.5, 2, 2.5, 2.75, 3.25$ is varied for $(c), (e), (g), (i), (k)$. The phases shown in snapshots c, e, g, i, k are crystalline (Cr), percolating network (P_n), elongated clusters (E), (E) but with shorter clusters, and aggregates (A), respectively. The volume fraction of NPs in (a) is 0.21 (2712 NPs), for c, e, g, i, k the NP-density is $0.38, 0.17, 0.092, 0.061, 0.018$, respectively.

Nano-particles of diameter σ_n interact with each other by the LJ potential suitably truncated at $2.5\sigma_n$ and the interaction energy is ϵ_n. The repulsive interaction between a NP and a monomer is given by the (suitably shifted) LJ-potential $V_{4n} = \epsilon_{4n}[(\sigma_{4n}/r_n)^{12} - (\sigma_{4n}/r_n)^6]$, $\forall r_n < 2^{1/6}\sigma_{4n}$, where $\epsilon_{4n} = 30k_BT$ and r_n is the NP-monomer distance. We keep all the WM-chain parameters fixed and vary only the EV diameter σ_{4n} between WM and NP, and σ_n.

We perform grand canonical MC (GCMC) simulations with the number of monomers fixed, but with an energy gain (loss) of $-\mu n_p(\mu n_p)$ for n_p added (removed) NPs is the simulation box; μ is the chemical potential. The equilibrium phase of the micelles and NPs is the phase separated structure as seen in Fig. 3a and b for low densities of particles with $\mu = -0.48k_BT$, 4800 monomers, $\sigma_{4n} = 1.75\sigma$, $\sigma_n = 2\sigma$ and $\epsilon_n = 10k_BT$. By virtue of periodic boundary conditions, one can discern that there is only one single phase separated aggregate of monomeric chains. For denser systems with $\mu > 0$, 6800 monomers and $\epsilon_n = 14k_BT$, we observe aggregation of NPs between WM-stacks. However, kinetic barriers in these dense glassy systems are too high to enable the system to completely phase separate, but GCMC steps for

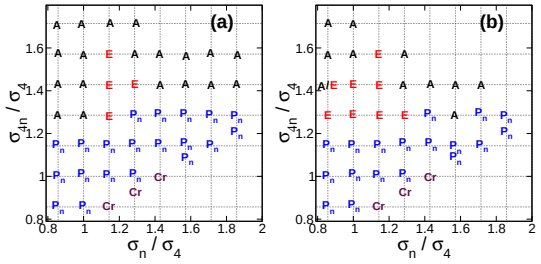

FIG. 4. The chart denoting the different dynamically arrested nano-structures formed as we change σ_{4n} and σ_n for $\epsilon_n = 14k_BT$ and (*a*) $\mu = 16k_bT$, (*b*) $\mu = 8k_bT$. Refer Fig. 3 for nano-structures nomenclature.

NPs help overcome local energy barriers enabling them to form aggregates: dynamically arrested phase separating structures. Within 10^6 MC steps, the structure of NP-aggregates within the micellar matrix gets nearly fixed, with slow changes in energy (less than 2.5%) and addition of only ~ 100 NPs over the next 10^6 MC steps [54].

In Figure 3 we show representative snapshots of self-assembled nano-structures formed by the aggregates of NPs in a matrix of nematically ordered WM chains. We keep $\epsilon_n = 14k_bT$, $\mu = 16k_BT$ and the NP radius $\sigma_n = 2\sigma$ of NPs fixed, and gradually increase the excluded volume parameter σ_{4n} of the monomer-NP interaction. At the lowest value of $\sigma_{4n} = 1.5\sigma$ (Fig.3*c*, *d*), we get a phase where the NPs are arranged in a periodic manner separated by chains of WM monomers. The monomers and NP form crystalline domains (Cr) with alternate positions of NP and monomer chains. We calculated the structure factors for NPs which confirm a crystalline structure (refer [54]). This phase occurs whenever the condition $\sigma/2 + \sigma_n/2 = \sigma_{4n}$ is satisfied. *Moreover*, enough free volume should be available for the NPs to fill up all the possible lattice sites. The free volume is dependent on both σ_{4n} and σ_n as well on the number density ρ of monomers. We have fixed ρ at $0.126\sigma^{-3}$ and σ_4 at 1.75σ, but the number of NPs can adjust to fill up the available space between WM chains. For other combinations of σ_{4n} and σ_n, we get near perfect lattice arrangement of NPs; the reader can confirm this in [54].

If now σ_{4n} is increased to 2σ from 1.75σ, a new structural arrangement of NPs is formed where the NPs start to phase separate to form percolating clusters of NPs which span throughout the system: refer Fig.3*e* and *f*. Kinetic trapping prevents complete phase separation, and we observe NP clusters separated by stacks of WM chains lead to morphologies which is akin percolating network (P_n) of NPs. If the WM phase was dissolved away at the end of the P_n formation as in [48, 49], a porous scaffold of NP micro-structure would be retained similar to what is seen in Fig.3f. Increase of σ_{4n} will lead to elongated structures conjoined at fewer points in space with fewer NPs in the system, and finally at $\sigma_{4n} = 2.5\sigma$, we have even fewer NPs which now form non-percolating elongated clusters (E) of NPs spanning the $\hat{z}$ direction: refer Fig.3*g* and *h*. Clusters grow along the nematic direction to minimize elastic energy costs paid by nematically ordered WMs to accomodate NP clusters. A further increase in the value of σ_{4n} to 2.75σ leads to shorter and thinner elongated structures as shown in Fig.3*i* and *j*. Finally, small aggregates (A) dispersed in nematic matrix are found for even larger values of $\sigma_{4n} = 3.25$ some of which are rod like, as seen in Fig. 3*k* and *l*. For further increase in σ_{4n}, it is not possible to introduce NPs in the nematic matrix. The decrease in number of NPs as we change σ_{4n} is shown in [54].

The chart in Fig.4*a* and *b* summarizes the dynamically arrested nano-structures that we get as we systematically vary σ_{4n} and σ_n for two values of μ, viz, $\mu = 16k_BT$ and $\mu = 8k_BT$. The quantities σ_{4n} and σ_n have been normalized by $\sigma_4 = 1.75\sigma$. We have chosen σ_{4n} (the EV separation between NP and micellar chain), to be different from σ_4 (the EV separation between two parallel chains of WM) to have an independent handle on changing NP-WM interactions keeping the volume fraction of micellar chains fixed. In an experimental realization, σ_{4n} could be different from that of σ_4 due to differences in microscopic interactions [48]. We ensure that σ_{4n} is such that $\sigma_{4n} \geq (\sigma + \sigma_n)/2$. As mentioned before, we get Cr arrangement of NPs when the condition $\sigma_{4n} = (\sigma+\sigma_n)/2$ is satisfied. At times, the lattice arrangement does not span the system and forms crystalline domains instead. We get perfect crystal structures for $\epsilon_n = 30k_BT$, see [54]. As σ_{4n} is increased, we get the P_n phase and then the A phase for all values of σ_n, but there also exists an island of elongated clusters of NPs (E) in the phase diagram. For certain parameter values, these elongated clusters are perfectly rod like, refer [54].

In summary, we have used semi-grand-canonical simulations to demonstrate the aggregation and growth of nanoparticle clusters with different morphologies. The NP clusters get dynamically arrested within self-assembled chains of semiflexible worm-like micelles. The different nanostructures obtained are (a) a crystalline arrangement of NPs and monomers, (b) percolating networks of aggregated NPs creating a porous structure, (c) elongated rod like structures of NPs of variable length and aspect ratios, and (d) smaller clusters of different shapes and sizes. In contrast to systems theoretically investigated previously, our choice of the size and densities of NPs are such that NP clusters and micellar matrix mutually affect and modify each other's local morphology and structure. We can get different nano-structures by varying μ of NPs, the EV of micellar chains seen by NPs as well as the NP radius. In future we plan to vary monomer density as well.

AC acknowledges the use of the compute-cluster of Nano-Science unit in IISER, funded by DST, India by project no. SR/NM/NS-42/2009. AC thanks K. Guruswamy for very useful discussions.

* apratim@iiserpune.ac.in

[1] D. Frenkel and D. J. Wales, Nature Materials **10**, 410 (2011).

[2] T. Curk, F. J. Martinez-Veracoechea, D. Frenkel, and J. Dobnikar, Nano Letters **14**, 2617 (2014).

[3] W. A. Lopes and H. M. Jaeger, Nature **414**, 735 (2001).

[4] G. Whitesides, J. Mathias, and C. Seto, Science **254**, 1312 (1991).

[5] P. J. Lu, E. Zaccarelli, F. Ciulla, A. B. Schofield, F. Sciortino, and D. A. Weitz, Nature **453**, 499 (2008).

[6] E. Zaccarelli, P. J. Lu, F. Ciulla, D. A. Weitz, and F. Sciortino, Journal of Physics: Condensed Matter **20**, 494242 (2008).

[7] T. Araki and H. Tanaka, Physical Review Letters **97**, 127801 (2006).

[8] V. Shchukin and D. Bimberg, Reviews of Modern Physics **71**, 1125 (1999).

[9] B. Charleux, G. Delaittre, J. Rieger, and F. DAgosto, Macromolecules **45**, 6753 (2012).

[10] Zhenli and S. C. Glotzer, Nano Letters **4**, 1407 (2004).

[11] M. Grzelczak, J. Vermant, E. M. Furst, and L. M. Liz-Marzn, ACS Nano **4**, 3591 (2010).

[12] J. K. Whitmer, A. A. Joshi, T. F. Roberts, and J. J. de Pablo, Journal of Chemical Physics **138**, 194903 (2013).

[13] J. A. Moreno-Razo, E. J. Sambriski, N. L. Abbott, J. P. Hernandez-Ortiz, J. J. de Pablo, Nature **48**, 86 (2012).

[14] J. K. Whitmer, X. Wang, F. Mondiot, D. S. Miller, N. L. Abbott, and J. J. de Pablo, Physical Review Letters **111**, 227801 (2013).

[15] V. K. N. Gupta, A. Mehra, and R. Thaokar, Colloids and Surfaces A: Physicochemical and Engineering Aspects **393**, 73 (2012).

[16] M. Grzelczak, Jan Vermant, Eric M. Furst, and Luis M. Liz-Marzan, ACS Nano Review, **4**, 3591 (2010).

[17] Carlos-Andres Palma, M. Cecchini and P. Samori, Chem. Soc. Rev., **41**, 37133730 (2012).

[18] YongJoo Kim and A. Alexander-Katz, J. Chem. Phys. **135**, 024902 (2011).

[19] F. W. Starr, Jack F. Douglas, and S. C. Glotzer, J. Chem. Phys. **119**, 1777 (2003).

[20] V. Pryamtisyn, Venkat Ganesan, A. Z. Panagiotopoulos, Hongjun Liu, and Sanat K. Kumar, J. Chem. Phys. **131**, 221102 (2009).

[21] J. R. Spaeth, I. G. Kevrekidis, and A. Z. Panagiotopoulos, J. Chem. Phys. **135** , 184903 (2011)

[22] A. J. Rahedi, Jack F. Douglas, and F. W. Starr, J. Chem. Phys. **128**, 024902 (2008)

[23] Ethayaraja M., E. Sanz, S. Roy, M. Dijkstra, Jan Groenewold, W. K. Kegel, J. Chem. Phys. 136, 144706 (2012);

[24] Z.-W. Li, Z.-Y. Lu, Z.-Y. Sun, and L.-J. An, Soft Matter **8**, 6693 (2012).

[25] M. A. Horsch, Z. Zhang, and S.C. Glotzer, Physical Review Letters **95**, 056105 (2005).

[26] B. A. Parviz, D. Ryan, and G. M. Whitesides, IEEE Transactions on Advanced Packaging **26**, 233 (2003).

[27] G. A. Ozin, K. Hou, B. V Lotsch, L. Cademartiri, D.P. Puzzo, F. Scotognella, A. Ghadimi, J. Thomson, Materials Today **12**, 12 (2009).

[28] E. Leontidis, M. Orphanou, T. Kyprianidou-Leodidou, F. Krumeich, and W. Caseri, Nano Letters **3**, 569 (2003).

[29] M. A. Gharbi, M. Nobili, and C. Blanc, Journal of Colloid and Interface Science **417**, 250 (2014).

[30] M. Zapotocky, L. Ramos, P. Poulin, T. C. Lubensky, D. A. Weitz, Science **283**, 209 (1999).

[31] P. Poulin, H. Stark, T. C. Lubensky, D. A. Weitz, Science **275**, 1770 (1997).

[32] L. Ramos, T. C. Lubensky, N. Dan, Philip Nelson and D. A. Weitz, Science **286**, 2325 (1999).

[33] B. Senyuk, Q. Liu, S. He, R. D. Kamien, R. B. Kusner, T. C. Lubensky, and I. I. Smalyukh, Nature **493**, 200 (2013).

[34] J.I. Fukuda and S. Zumer, Physical Review E **79**, 041703 (2009).

[35] J.H. McCoy, W. Brunner, W. Pesch, and E. Bodenschatz, Physical Review Letters **101**, 254102 (2008).

[36] I. Musevic and M. Skarabot, Soft Matter **4**, 195 (2008).

[37] M. Ravnik and S. Zumer, Soft Matter **5**, 269 (2009).

[38] U. Tkalec, M. Ravnik, S. Zumer, and I. Musevic, Physical Review Letters **103**, 127801 (2009).

[39] M. Skarabot, M. Ravnik, S. Zumer, U. Tkalec, I. Poberaj, D. Babic, and I. Musevic, Phys. Rev. E **77**, 061706 (2008).

[40] C. Zhou, P. Yue and J. J. Feng, Langmuir, **24**, 3099 (2008).

[41] H. Stark, Physics Reports **351**, 387 (2001)

[42] K. P. Sharma, V. K. Aswal, and G. Kumaraswamy, Journal of Physical Chemistry B **114**, 10986 (2010).

[43] K. P. Sharma, A. K. Ganai, S. Sen Gupta, and G. Kumaraswamy, Chemistry of Materials **23**, 1448 (2011).

[44] K. P. Sharma, G. Kumaraswamy, I. Ly, and M. M. Olivier, Journal of Physical Chemistry B **113**, 3423 (2009).

[45] M. E. Cates and S. J. Candau, Journal of Physics: Condensed Matter **2**, 6869 (1999).

[46] J.F. Berret, arXiv:cond-mat/0406681v1.

[47] S. Lerouge, J.F. Berret, arXiv:0910.1854v1.

[48] T. Hegmann, H. Qi and V. M. Marx, Journal of Inorganic and Organometallic Polymers and Materials, **17**, 483 (2007).

[49] C. Wang, D. Chen and X. Jiao, Sci. Technol. Adv. Mater. **10** 023001 (2009).

[50] A. Chatterji, R. Pandit, Europhys. Lett. **54**, 213 (2001).

[51] A. Chatterji, R. Pandit, J. of Stat. Phys., **110**, 1219, (2003)

[52] K. R. Prathyusha, A. P. Deshpande, M. Laradji, and P. B. Sunil Kumar, Soft Matter **9**, 9983 (2013).

[53] Snigdha Thakur, Prathyusha K. R., Abhijit P. Deshpande, Mohamed Laradji and P. B. Sunil Kumar, Soft Matter **60**, 489 (2010).

[54] Refer Supplementary Material for supporting figures.